Inorg. Chem. **2007**, *46*, 10153–10157

Magnetic Interaction of Tri- and Di-oxytriphenylamine Radical Cation $FeCl_4$ Salts

Masato Kuratsu, Shuichi Suzuki, Masatoshi Kozaki, Daisuke Shiomi,* Kazunobu Sato, Takeji Takui, and Keiji Okada*

Departments of Chemistry and Materials Science, Graduate School of Science, Osaka City University, Sugimoto, Sumiyoshi-ku, Osaka 558-8585, Japan

Received June 27, 2007

The tetrachloroferrates of the 2,2′:6′,2″:6″,6-trioxytriphenylamine ($TOT^{\cdot+}$•$FeCl_4^-$) and 2,2′:6′,2″-dioxytriphenylamine ($DOT^{\cdot+}$•$FeCl_4^-$) radical cations were prepared, and their structures, magnetic properties, and the relationship between them were investigated. The $TOT^{\cdot+}$ moiety had a highly planar structure and packed as a dimer surrounded by tetrachroferrates, which also formed a dimer structure. The magnetic properties of $TOT^{\cdot+}$•$FeCl_4^-$ were characterized by strong ($2J/k_B = \sim -1.3 \times 10^3$ K, $H = -2J\mathbf{S}_{1/2}\cdot\mathbf{S}_{1/2}$) and weak ($2J/k_B = -1.76$ K, $H = -2J\mathbf{S}_{5/2}\cdot\mathbf{S}_{5/2}$) antiferromagnetic interactions due to the $(TOT^{\cdot+})_2$ and $(FeCl_4^-)_2$ structures, respectively. $DOT^{\cdot+}$ had a twisted form and no dimer formation was observed between the $DOT^{\cdot+}$'s and $FeCl_4^-$'s. Instead, short contacts between the $DOT^{\cdot+}$ and chlorine atoms and between the $DOT^{\cdot+}$'s producing a $DOT^{\cdot+}$ chain were observed. The magnetic properties of $DOT^{\cdot+}$•$FeCl_4^-$ were characterized by a 3D magnetic phase transition to an antiferromagnet with $T_N = \sim 8$ K.

Introduction

There has been much interest in the magnetic properties of organic (radicals or radical ions) and inorganic (magnetic metal ions) and their composite materials.[1] A recent development of molecule-based magnets has demonstrated a variety of magnetic interactions exhibiting interesting magnetic properties and has also provided an important insight into the relationship between the magnetic properties and crystal packing structures. Of the various magnetic materials, antiferromagnets have been observed in some neutral radicals.[2] More recently, TTF-based radical cations were shown to be transformed into antiferromagnets at low temperature through a $\pi-$d interaction with magnetic metal ions.[3] Related studies regarding radical cations other than TTF derivatives and a well-known example of Wurster's blue perchlorate[4] are extremely sparse.[5] The antiferromagnets are in three-dimensionally spin-ordered states and can be differentiated from the materials showing low-dimensional antiferromagnetic interactions. Although it is quite difficult to predict at the molecular design level as to whether the materials show magnetic ordering or not at low temperature, we have envisioned that low-dimensional magnetic interactions might

* To whom correspondence should be addressed. E-mail: okadak@sci.osaka-cu.ac.jp, Tel: +81-6-6605-2568, Fax: +81-6-6690-2709 (K.O.), E-mail: shiomi@sci.osaka-cu.ac.jp (D.S.).

(1) (a) Kahn, K. *Molecular Magnetism*; VCH Publishers: New York, 1993. (b) *Magnetic Properties of Organic Materials*; Lahti, P. M., Ed.; Marcel Dekker: New York, 1999. (c) *Magnetism: Molecules to Materials II-V*; Miller, J. S., Drillon, M., Eds.; Wiley-VCH: New York, 2001−2005.

(2) For examples, (a) Awaga, K.; Tanaka, T.; Shirai, T.; Fujimoto, M.; Suzuki, Y.; Yoshikawa, H.; Fujita, W. *Bull. Chem. Soc. Jpn*. **2006**, *79*, 25−34. (b) Hayakawa, K.; Shiomi, D.; Ise, T.; Sato, K.; Takui, T. *J. Phys. Chem. B* **2005**, *109*, 9195−9197. (c) Takeda, K.; Yoshida, Y.; Inanaga, Y.; Kawase, T.; Shiomi, D.; Ise. T.; Kozaki, M.; Okada, K.; Sato, K.; Takui, T. *Phys. Rev. B* **2005**, *72*, 024435-1-024435-6. (d) Miyazaki, Y.; Sakakibara, T.; Ferrer, J. R.; Lahti, P. M.; Antorrena, G.; Palacio, F.; Sorai, M. *J. Phys. Chem. B* **2002**, *106*, 8615−8620. (e) Sutter, J-P.; Daro, N.; Golhen, S.; Ouhab, L.; Oliver, K. *Mol. Cryst. Liq. Cryst.* **1999**, *334*, 69−79. (f) Takizawa, O. *Bull. Chem. Soc. Jpn*. **1976**, *49*, 583−588. (g) Yamaguchi, J. *Chem. Lett*. **1972**, 733−735. (h) Duffy, W.; Duback, J. F.; Pinetta, P. A.; Deck, J. F.; *J. Chem. Phys.* **1972**, *56*, 2555−2561.

(3) (a) Miyazaki, A.; Yamazaki, H.; Enoki, T.; Watanabe, R.; Ogura, E.; Kuwatani, Y.; Iyoda, M. *Inorg. Chem*. **2007**, *46*, 3353−3366. (b) Shirahata, T.; Kibune, M.; Maesato, M.; Kawashima, T.; Saito, G.; Imakubo, T. *J. Mater. Chem*. **2006**, *16*, 3381−3390. (c) Miyazaki, A.; Umeyama, T.; Enoki, T.; Ogura, E.; Kuwatani, Y.; Iyoda, M.; Nishikawa, H.; Ikemoto, I.; Kikuchi, *Mol. Cryst. Liq. Cryst.* **1999**, *334*, 379−388. (d) Umeya, K., M.; Kawata, S.; Matsuzaka, H.; Kitagawa, S.; Nishikawa, H.; Kikuchi, K.; Ikemoto, I. *J. Mater. Chem.* **1998**, *8*, 295−300.

(4) (a) Duffy, W., Jr. *J. Chem. Phys.* **1962**, *36*, 490−493. (b) Okumura, K. *J. Phys. Soc. Jpn.* **1963**, *18*, 69−73. (c) Chihara, H.; Nakamura, M.; Seki, S. *Bull. Chem. Soc. Jpn*. **1965**, *33*, 1776−1778. (d) Chesnut, D. B. *J. Chem. Phys.* **1966**, *45*, 4677−4681. (e) Soos, Z. G.; Hughes, R. C. *J. Chem. Phys.* **1967**, *46*, 253−259. (f) Tanaka, J.; Inoue, M.; Mizuno, M.; Horai, K. *Bull. Chem. Soc. Jpn*. **1970**, *43*, 1998−2002. (g) Awano, H.; Araki, H.; Ohigashi, H. *Synth. Met.* **1993**, *55−57*, 685−689.

10.1021/ic7012649 CCC: $37.00
Published on Web 10/31/2007

be altered to higher-dimensional interactions by modifying the organic spin structure into a higher-dimensional structure.

During the course of our study to develop multispin systems,[6] we have recently prepared 2,2′:6′,2″:6″,6-trioxytriphenylamine (TOT)[7] and 2,2′:6′,2″-dioxytriphenylamine (DOT),[8] which have low oxidation potentials (+0.11 V vs Fc/Fc^+ for TOT and +0.33 V for DOT) and provide stable radical cations (PF_6 salts).[7] The molecular structure of $TOT^{\cdot+}$ is highly planar, whereas that of $DOT^{\cdot+}$ is expected to be twisted because of the steric repulsion between the two-edge phenyl rings. Because of the potential stability of these oxygen-bridged radical cations without bulky substituents, the magnetic interactions between the radical cations and the counter anions can be expected, depending on the crystal packing structures. We report the preparation and magnetic properties of $TOT^{\cdot+}\cdot FeCl_4^-$ and $DOT^{\cdot+}\cdot FeCl_4^-$, the latter of which exhibits a 3D magnetic phase transition into an antiferromagnet at ca. 8 K.

Experimental Section

The chemicals were of commercial grade and were used without further purification. Melting points were measured using a Yanako MP-J3 apparatus, and they are not corrected. The infrared spectra were measured using a Shimadzu FTIR-8700. The EPR spectra were recorded by a Brucker ELEXSYS E500. The X-ray data were collected by a Rigaku CCD area detector with graphite monochromated Mo Kα radiation. The structures were solved by a direct method (*SIR92* or *SHELX97*), and they were expanded using a Fourier technique. All of the calculations were performed using the *Crystal Structure* crystallographic software package. The magnetic susceptibility measurements were performed using a Quantum Design SQUID magnetometer, MPMS-XL.

Synthesis of Thianthrene$^{\cdot+}\cdot FeCl_4^-$. The oxidation of thianthrene was carried out in an electrochemical cell, which has two compartments (each 25 cm^3) separated by a glass filter and equipped with platinum electrodes (15 × 15 mm^2). An elelctrolyte solution of tetra-*n*-butylammonium tetrachloroferrate (973 mg, 2.21 mmol) in dichloromethane (50 cm^3) was prepared. Half of the solution was added to the cathodic compartment in the cell. Thianthrene (393 mg, 1.82 mmol) was dissolved in the remaining electrolyte solution, and this solution was added to the anodic compartment. Both compartments in the cell were purged with argon for a few minutes. The electrolysis was carried out at a constant current (1.0 mA) using a galvanostat. After a few minutes, the color of the solution on the anodic side turned purple. After 1 day, purple crystals had deposited on the platinum surface. These crystals were repeatedly collected several times (408 mg, 54% after third cycle). Thus, the prepared thianthrene tetrachloroferrate was pure enough, as confirmed by an elemental analysis. Thinathrene$^{\cdot+}\cdot FeCl_4^-$ ($C_{12}H_8Cl_4FeS_2$), fw 413.98; deep-purple blocks; mp ca. 209 °C (decomp); EPR (powder) $g = 2.0125$ as a broad and monotonic signal with a width of 134 G at half-height; MS (FAB^+): *m*/*z* 216 [$C_{12}H_8S_2^+$], (FAB^-): *m*/*z* 198 [$FeCl_4^-$]; IR (KBr) ν_{max}/cm^{-1}: 1541, 1518, 1452, 1439, 1431, 1418, 1304, 1259, 1250, 1101, 1024, 762, 750, 660; Anal. Calcd for $C_{12}H_8Cl_4FeS_2$: C, 34.82; H, 1.95. Found: C, 34.96; H, 1.83.

Table 1. Crystallographic Data of $TOT^{\cdot+}\cdot FeCl_4^-$ and $DOT^{\cdot+}\cdot FeCl_4^-$

	$TOT^{\cdot+}\cdot FeCl_4^-$	$DOT^{\cdot+}\cdot FeCl_4^-$
formula	$C_{18}H_9Cl_4FeNO_3$	$C_{18}H_{11}Cl_4FeNO_2$
fw	484.93	470.95
cryst syst	monoclinic	monoclinic
space group	*C*2/*c* (#15)	$P2_1/c$ (#14)
a (Å)	22.743(6)	9.9281(19)
b (Å)	12.608(3)	13.089(2)
c (Å)	16.053(4)	15.659(3)
β (deg)	129.009(3)	112.120(4)
V (Å^3)	3576.8(14)	1885.1(6)
Z	8	4
cryst size (mm^3)	0.25 × 0.20 × 0.20	0.30 × 0.30 × 0.15
T (K)	113	113
D_{calcd} (g cm^{-3})	1.801	1.659
F(000)	1936.00	944.00
μ (cm^{-1})	14.591 (Mo Kα)	13.777 (Mo Kα)
reflns measured	17 245	17 635
unique reflns	3967	4220
observation	2876 ($I > 2\sigma(I)$)	3525 ($I > 2\sigma(I)$)
variables	253	246
R_1 [$I > 2\sigma(I)$][a]	0.041	0.033
R_w[b]	0.044	0.037
GOF	1.00	1.00

[a] $R_1 = \sum||F_o| - |F_c||/\sum|F_o|$. [b] $R_w = [\sum w(|F_o| - |F_c|)^2/\sum wF_o^2]^{1/2}$.

Synthesis of Thianthrene$^{\cdot+}\cdot GaCl_4^-$. The same method was employed for the preparation of the $GaCl_4^-$ salt. Using tetra-*n*-butylammonium tetrachlorogallate (1.00 g, 2.21 mmol) in dichloromethane (50 cm^3) as an electrolyte solution and thianthrene (393 mg, 1.82 mmol), thianthrene$^{\cdot+}\cdot GaCl_4^-$ was obtained in a similar yield (396 mg, 51% yield after third cycle). Thinathrene$^{\cdot+}\cdot GaCl_4^-$ ($C_{12}H_8Cl_4GaS_2$), fw 427.86; deep-purple blocks; mp ca. 215 °C (decomp), EPR (powder) $g = 2.0080$ as three-line signals with anisotropy of *g* factor ($g_{xx} = 2.0140$, $g_{yy} = 2.0081$, $g_{zz} = 2.0018$); MS (FAB^+): *m*/*z* 216 [$C_{12}H_8S_2^+$], (FAB^-): *m*/*z* 211 [$GaCl_4^-$]; IR (KBr) ν_{max}/cm^{-1}: 1541, 1518, 1508, 1439, 1433, 1418, 1306, 1261, 1250, 1101, 1026, 762, 752; Anal. Calcd for $C_{12}H_8Cl_4GaS_2$: C, 33.69; H, 1.88. Found: C, 33.39; H, 1.84.

Synthesis of $TOT^{\cdot+}\cdot FeCl_4^-$. The following procedure was carried out in a glove box. To a solution of TOT (74.4 mg, 0.259 mmol) in dichloromethane (50 cm^3) was added a solution of thianthrene$^{\cdot+}\cdot FeCl_4^-$ (107 mg, 0.258 mmol) in acetonitrile (50 cm^3) at room temperature. After stirring for 30 min, the solvent was removed under reduced pressure. The residue was dissolved in a minimum amount (4 cm^3) of acetonitrile. Diethyl ether (50 cm^3) was then added to the acetonitrile solution. $TOT^{\cdot+}\cdot FeCl_4^-$ was obtained as a green precipitate (102 mg, 81% yield). This compound was recrystallized from acetonitrile−diethyl ether as follows: $TOT^{\cdot+}\cdot FeCl_4^-$ was dissolved in acetonitrile in a small round flask. The flask was placed in a larger bottle containing diethyl ether. The bottle was capped and kept at room temperature for 1 day, which produced a single-crystal suitable for X-ray structure analysis. $TOT^{\cdot+}\cdot FeCl_4^-$, deep-green blocks from acetonitrile−diethyl ether, mp ca. 288 °C (decomp), IR (KBr) ν_{max}/cm^{-1} 3074, 1607, 1589, 1501, 1333, 1275, 1159, 1072, 1028, 893, 787, 721, 554. Anal. Found: C, 44.55; H, 1.76; N, 2.83. Calcd for $C_{18}H_9Cl_4FeNO_3$: C, 44.58; H, 1.87; N, 2.89. EPR (powder) $g = 2.0252$ as a broad and monotonic signal with a width of 135 G at half-height. Crystallographic data for $TOT^{\cdot+}\cdot FeCl_4^-$ are listed in Table 1, CCDC 643796.

(5) (a) Clerac, R.; Fourmigue, M.; Coulon, C. *J. Solid State Chem.* **2001**, *159*, 413−419. (b) Clerac, R.; Fourmigue, M.; Gaultier, J.; Barrans, Y.; Albouy, P. A.; Coulon, C. *Eur. Phys. J. B* **1999**, *9*, 431−443, 445−449. (c) Nishikawa, H.; Sekiya, H.; Fujiwara, A.; Kodama, T.; Ikemoto, I.; Kikuchi, K.; Yamada, J-I.; Oshio, H.; Kobayashi, K.; Yasuzaka, S.; Murata, K. *Chem. Lett.* **2006**, *35*, 912−913.
(6) Hiraoka, S.; Okamoto, T.; Kozaki, M.; Shiomi, D.; Sato, K.; Takui, T.; Okada, K. *J. Am. Chem. Soc.* **2004**, *126*, 58−59.
(7) Kuratsu, M.; Kozaki, M.; Okada, K. *Angew. Chem., Int. Ed.* **2005**, *44*, 4056−4058.
(8) Kuratsu, M.; Kozaki, M.; Okada, K. *Chem. Lett.* **2004**, *33*, 1174−1175.

Synthesis of $TOT^{\cdot+}\cdot GaCl_4^-$. This salt was prepared in the same manner as for $TOT^{\cdot+}\cdot FeCl_4^-$ except that thianthrene$^{\cdot+}\cdot GaCl_4^-$ was used instead of thianthrene$^{\cdot+}\cdot FeCl_4^-$. $TOT^{\cdot+}\cdot GaCl_4^-$ was obtained in 81% yield and recrystallized from acetonitrile−diethyl ether as described above. $TOT^{\cdot+}\cdot GaCl_4^-$, deep-green blocks from acetonitrile−diethyl ether, mp >300 °C, IR (KBr) ν_{max}/cm^{-1} 3076, 1609, 1589, 1501, 1333, 1275, 1159, 1072, 1028, 893, 787, 721, 554. Anal. Found: C, 43.54; H, 1.94; N, 2.65. Calcd for $C_{18}H_9Cl_4GaNO_3$: C, 43.34; H, 1.82; N, 2.81. EPR (powder) $g = 2.0040$ as a monotonic signal with a width of 4.7 G at half-height. Crystallographic data for $TOT^{\cdot+}\cdot GaCl_4^-$ ($C_{18}H_9Cl_4GaNO_3$); fw 498.80, monoclinic, space group $C2/c$ (# 15), $a = 22.738(6)$, $b = 12.651(2)$, $c = 17.862(5)$ Å, $\beta = 135.614(5)°$, $V = 3594.1(14)$ Å^3, $Z = 8$, $T = 113$ K, unique reflections 4037, observations 3430 ($I > 2\sigma(I)$), $R_1 = 0.031$, $R_w = 0.036$ [$I > 2\sigma(I)$], CCDC 643797.

Synthesis of $DOT^{\cdot+}\cdot FeCl_4^-$. This salt was prepared in the same manner as for $TOT^{\cdot+}\cdot FeCl_4^-$. $DOT^{\cdot+}\cdot FeCl_4^-$ was obtained in 82% yield. Single crystals were obtained by recrystallization as follows: $DOT^{\cdot+}\cdot FeCl_4^-$ was dissolved in dichloromethane in a small round flask. Hexane was carefully placed on the dichloromethane solution. The flask was capped and kept at room temperature for 1 day to give single crystals for X-ray analysis. $DOT^{\cdot+}\cdot FeCl_4^-$, $C_{18}H_{11}Cl_4FeNO_2$, fw 470.94, deep-green blocks from dichloromethane−hexane, mp ca. 193 °C (decomp), IR (KBr) ν_{max}/cm^{-1} 3082, 1630, 1580, 1491, 1339, 1300, 1275, 1234, 1163, 1153, 1124, 1115, 1057, 862, 791, 760, 712, 600. Anal. Found: C, 45.99; H, 2.27; N, 2.95. Calcd for $C_{18}H_{11}Cl_4FeNO_2$: C, 45.91; H, 2.35; N, 2.97. EPR (powder) $g = 2.0165$ as a broad and monotonic signal with a width of 87 G at half-height. Crystallographic data for $DOT^{\cdot+}\cdot FeCl_4^-$ are listed in Table 1, CCDC 643794.

Synthesis of $DOT^{\cdot+}\cdot GaCl_4^-$. This salt was prepared in the same manner as for $TOT^{\cdot+}\cdot GaCl_4^-$. $DOT^{\cdot+}\cdot GaCl_4^-$ was obtained in 75% yield and recrystallized from dichloromethane−hexane as described above. $DOT^{\cdot+}\cdot GaCl_4^-$, $C_{18}H_{11}Cl_4GaNO_2$, fw 484.82, deep-green blocks from dichloromethane−hexane, mp ca. 216 °C (decomp), IR (KBr) ν_{max}/cm^{-1} 3084, 1630, 1582, 1491, 1337, 1300, 1277, 1234, 1163, 1153, 1124, 1115, 1057, 864, 791, 760, 712, 600. Anal. Found: C, 44.35; H, 2.39; N, 2.77. Calcd for $C_{18}H_{11}Cl_4GaNO_2$: C, 44.59; H, 2.29; N, 2.89. EPR (powder) $g = 2.0030$ as a monotonic signal with a width of 1.8 G at half-height. Crystallographic data for $DOT^{\cdot+}\cdot GaCl_4^-$ ($C_{18}H_{11}Cl_4GaNO_2$); fw 484.82, monoclinic, space group $P2_1/c$ (# 14), $a = 9.937(2)$, $b = 13.082(3)$, $c = 15.677(4)$ Å, $\beta = 112.065(4)°$, $V = 1888.8(7)$ Å,^{3} $Z = 4$, $T = 113$ K, unique reflections 4245, observations 3313 ($I > 2\sigma(I)$), $R_1 = 0.037$, $R_w = 0.040$ [$I > 2\sigma(I)$], CCDC 643795.

Results and Discussion

Syntheses of $FeCl_4^-$ and $GaCl_4^-$ Salts. $TOT^{\cdot+}\cdot FeCl_4^-$ ($GaCl_4^-$) and $DOT^{\cdot+}\cdot FeCl_4^-$ ($GaCl_4^-$) were successfully prepared in high yields by the addition of an acetonitrile solution of thianthrene$^{\cdot+}\cdot FeCl_4^-$ ($GaCl_4^-$) to a solution of neutral TOT or DOT in dichloromethane in a glove box (Scheme 1). Single crystals of $TOT^{\cdot+}\cdot FeCl_4^-$ ($GaCl_4^-$) and $DOT^{\cdot+}\cdot FeCl_4^-$ ($GaCl_4^-$) were obtained by recrystallization from acetonitrile−diethyl ether and dichloromethane−hexane, respectively. These radical cation salts were stable under aerated conditions at room temperature.

Structure of $TOT^{\cdot+}\cdot FeCl_4^-$. The X-ray structure of $TOT^{\cdot+}\cdot FeCl_4^-$ is shown in Figure 1. The crystallographic data are shown in Table 1. The bond lengths of N-Csp^2 were in the range of 1.377−1.383 Å and shorter than those

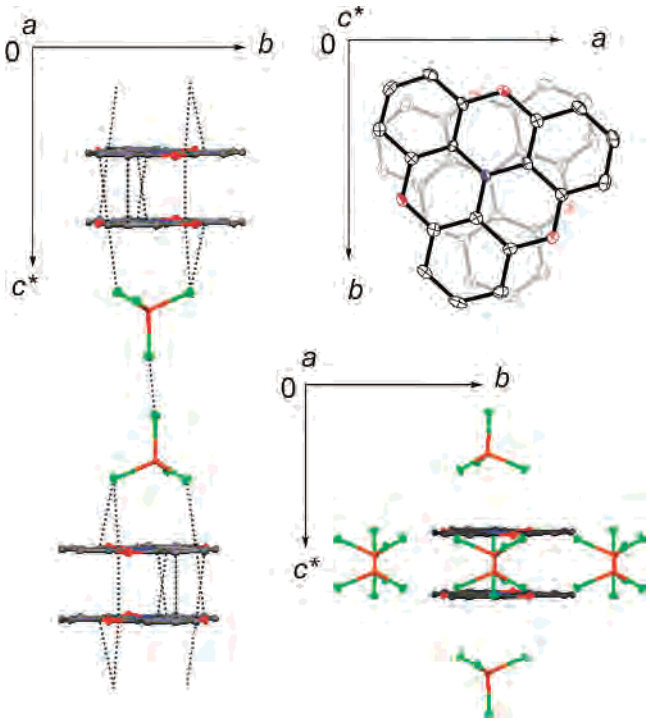

Figure 1. Crystal packing structures of $TOT^{\cdot+}\cdot FeCl_4^-$ projected along the *a* axis (left and bottom right) and *c** axis (top right); each axis shows only the direction, whereas the length is meaningless; the dotted lines show intermolecular short contacts; hydrogen atoms are omitted for clarity. Details of the short contacts including bond lengths are given in Table S1 in the Supporting Information.

Scheme 1

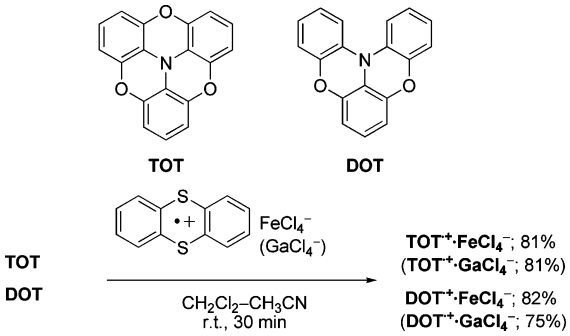

(1.404−1.411 Å) of the neutral TOT.[7] The $TOT^{\cdot+}$ moiety had a highly planar structure similar to the previously reported PF_6 salt. Several intermolecular contacts shorter than the van der Waals contact (aromatic C−C contact 3.54 Å)[9] were observed between the sp^2 carbon atoms (3.29−3.39 Å, shown as dotted lines in Figure 1, Table S1 in the Supporting Information), resulting in a $TOT^{\cdot+}$ dimer formation. The observed short contacts are most likely due to the crystal packing force. They are not in the range of the σ-bond formation because of the instability of the radical ion, as evidenced by the highly planar structure of $TOT^{\cdot+}$ without pyramidalization of the contacted carbon atoms. This consideration is supported by the crystal structure of the PF_6 salt, where no $TOT^{\cdot+}-TOT^{\cdot+}$ contact was observed.[7] The $TOT^{\cdot+}$ dimer was surrounded by eight $FeCl_4^-$ counter anions (Figure 1, bottom right). Additional short contacts were

(9) Bondi, A. *J. Phys. Chem.* **1964**, *68*, 441−451.

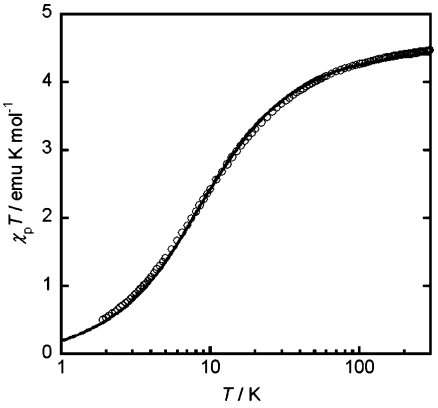

Figure 2. χ_pT-T plots of $TOT^{\cdot+}\cdot FeCl_4^-$ (powder) under a magnetic field of 1000 Oe; the temperature axis is plotted on a log scale for comparison with the simulation curve (solid line) based on the dimer model of $S = {}^5/_2$ using $2J/k_B = -1.76$ K.

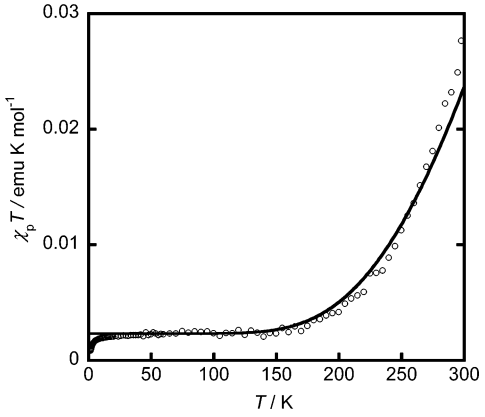

Figure 3. χ_pT-T plots for $TOT^{\cdot+}\cdot GaCl_4^-$ (powder) under a magnetic field of 3000 Oe and the simulation curve (solid line) with the ST model using parameters of $2J/k_B = -1250$ K and $g = 2.0040$ (powder EPR), in which a 0.62% impurity was assumed.

observed between the aromatic carbon atoms and chlorine atoms of $FeCl_4^-$ and also between the chlorine atoms of the $FeCl_4^-$ counter anions (Figure 1, left).

Magnetic Properties of $TOT^{\cdot+}\cdot FeCl_4^-$. The above short contacts would induce relatively strong antiferromagnetic interactions within the $TOT^{\cdot+}$ dimer and also between the $FeCl_4^-$ anions. The temperature dependence of χ_pT for $TOT^{\cdot+}\cdot FeCl_4^-$ is shown in Figure 2. The χ_pT value at room temperature was 4.47 emu K mol^{-1}, which is close to the theoretical value of $FeCl_4^-$ with $S = {}^5/_2$ and $g = 2.025$ ($\chi_pT = 4.49$ emu K mol^{-1}). There appears to be no contribution of $TOT^{\cdot+}$ ($S = {}^1/_2$), suggesting that the antiferromagnetic interaction within the $TOT^{\cdot+}$ dimer is much higher than 300 K. The χ_pT values decreased as the temperature was lowered, indicating a weak antiferromagnetic interaction between the $FeCl_4^-$ anions. The χ_pT values were reproduced using the parameter of $2J/k_B = -0.88$ K in the dimer model of $S = {}^5/_2$ ($H = -2J\mathbf{S}_{5/2}\cdot\mathbf{S}_{5/2}$) (Figure 2).

The antiferromagnetic interaction within the $TOT^{\cdot+}$ dimer was estimated using the $GaCl_4^-$ ($S = 0$) salt, which had a very similar structure belonging to the same space group. The χ_pT value of $TOT^{\cdot+}\cdot GaCl_4^-$ at room temperature was quite small (0.028 emu K mol^{-1}) and further decreased as the temperature was lowered. The simulation using the ST model with $2J/k_B = \sim -1.3 \times 10^3$ K assuming a 0.62% Curie impurity well reproduced the experimental results (Figure 3). Because of the similarity in the molecular and packing structures between the $FeCl_4^-$ and $GaCl_4^-$ salts, $TOT^{\cdot+}\cdot FeCl_4^-$ would have an antiferromagnetic interaction of a similar order, which may appear as a slight deviation between the observed and calculated χ_pT values in a high-temperature region ($T > 100$ K), as shown in Figure 2. Thus, the magnetic property of $TOT^{\cdot+}\cdot FeCl_4^-$ is characterized by a strong antiferromagnetic interaction within the dimer of the radical cations. The expected magnetic interaction between the radical cations and the counter anions was not visible because of the strong antiferromagnetic interaction induced by the dimer formation of the radical cations.

Structure of $DOT^{\cdot+}\cdot FeCl_4^-$. The twisted structure of $DOT^{\cdot+}$ would prevent dimer formation and may form a 3D spin network between the $DOT^{\cdot+}$ and $FeCl_4^-$ spins. Figure 4 shows the crystal packing structure of $DOT^{\cdot+}\cdot FeCl_4^-$. The crystallographic data are shown in Table 1. The bond lengths of the N-Csp^2 attached to the two-edge phenyl rings (1.402, 1.409 Å) were slightly longer than that (1.385 Å) attached to the central phenyl ring. The dihedral angle between the two-edged phenyl rings was 38.3° for the radical cation $DOT^{\cdot+}\cdot FeCl_4^-$. The value was slightly lower than that for the neutral state (43.0°).[8] The packing structure of $DOT^{\cdot+}\cdot FeCl_4^-$ was found to be a columnar alternating stack of $DOT^{\cdot+}$ and $FeCl_4^-$ along the b axis (Figure 4, Table S3 in the Supporting Information). A similar spin network was also observed along the a^* axis, producing a 2D network in the a^*-b plane. Furthermore, additional contacts were observed between the $DOT^{\cdot+}$s leading to a $DOT^{\cdot+}$ chain along the c axis (Figure 4, bottom). These contacts would lead to 3D antiferromagnetic interactions between the $DOT^{\cdot+}$ and $FeCl_4^-$ spins and

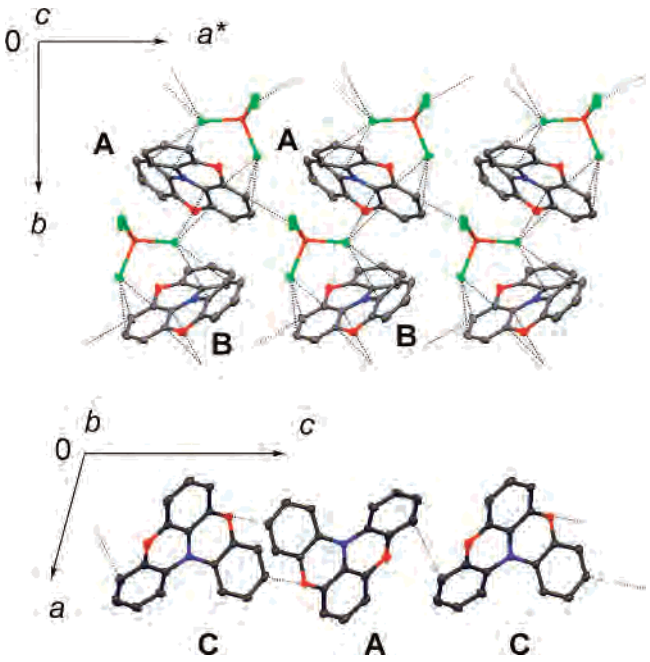

Figure 4. Crystal packing structures of $DOT^{\cdot+}\cdot FeCl_4^-$ projected along the c axis (top) and the b axis (bottom); each axis shows only the direction, whereas the length is meaningless; the dotted lines show intermolecular contacts; hydrogen atoms are omitted for clarity.

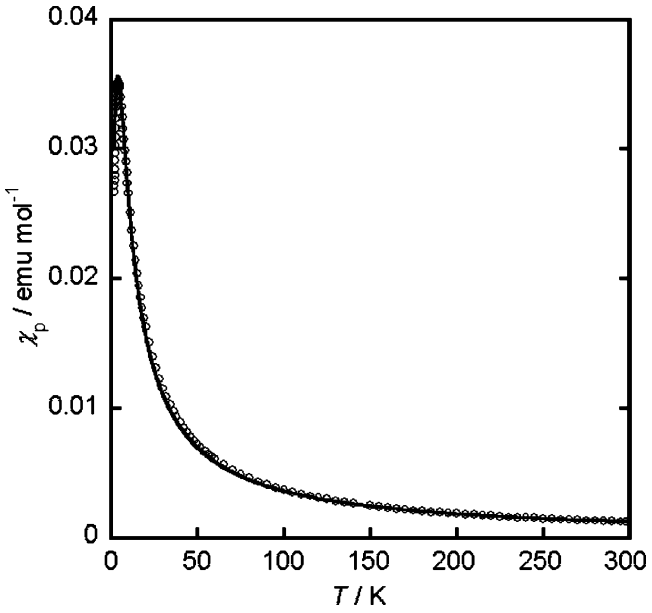

Figure 5. χ_p-T plots for $DOT^{\cdot+}\cdot GaCl_4^-$ (powder) under a magnetic field of 1000 Oe and a simulation line (solid line) based on Bonner−Fisher model using parameters $2J/k_B = -6.2$ K and $g = 2.0030$ (powder EPR), in which possible differences between the two magnetic interactions indicated from Figure 4 were neglected for simplicity.

between the $DOT^{\cdot+}$spins. No short contact between the chlorine atoms of $FeCl_4^-$ was observed.

Magnetic Properties of $DOT^{\cdot+}\cdot FeCl_4^-$. The magnetic interaction due to the short contacts leading to the $DOT^{\cdot+}$ chain was estimated from the measurement of the magnetic susceptibility of $DOT^{\cdot+}\cdot GaCl_4^-$ (Figure 5), which also had similar molecular and packing structures in the same space group as the $FeCl_4^-$ salt. The analysis was achieved by applying the Bonner−Fisher model[10] (eq 1), in which any possible difference in the magnetic interactions due to the different types of short contacts was neglected for simplicity.[11] The parameters $2J/k_B = -6.2$ K and $g = 2.0030$ (powder EPR) well reproduced the experimental values (Figure 5).

$$H = \sum_i [-2J\mathbf{S}^i\cdot\mathbf{S}^{i+1}] \qquad (1)$$

Figure 6 shows the χ_pT-T plots for $DOT^{\cdot+}\cdot FeCl_4^-$. The χ_pT value at room temperature was 4.77 emu K mol^{-1}, which is close to the summation of $S = {}^5/_2$ and $S = {}^1/_2$ using $g = 2.017$ (powder EPR). The χ_pT values gradually decreased as the temperature was lowered (r.t. → ca. 10 K). Further lowering of the temperature led to a sharp drop in the χ_pT values.

An insight into the sharp drop in χ_pT was obtained from an experiment using a single crystal of a suitable size (4.5 × 0.3 × 0.2 mm^3). The χ_p of the single crystal of

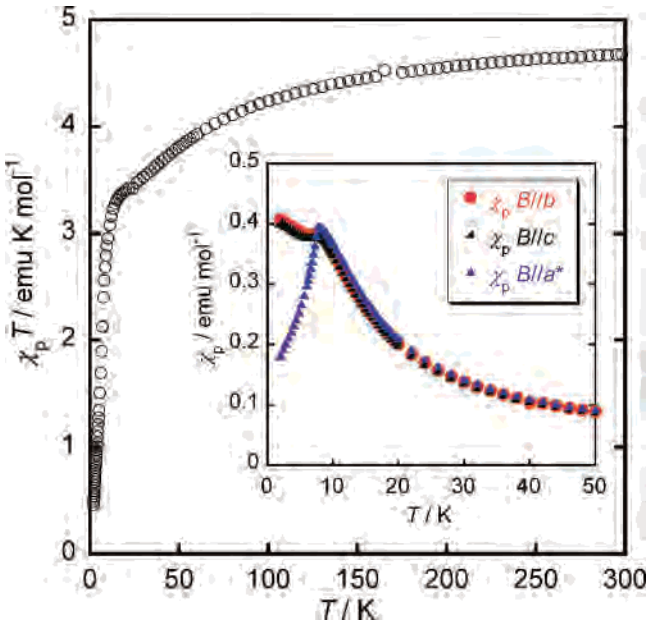

Figure 6. χ_pT-T plots for $DOT^{\cdot+}\cdot FeCl_4^-$ under a magnetic field of 1000 Oe; the inset shows χ_p-T plots for a single crystal with B//b, B//c, and B//a*.

$DOT^{\cdot+}\cdot FeCl_4^-$ was measured by applying a magnetic field B (50 mT) in three directions: B//a*, B//b, and B//c (inset of Figure 6). When the magnetic field was parallel to the b or c axes, B//b or B//c, the χ_p values were rather insensitive to the temperatures below 8 K. The temperature-independent susceptibility is typical for ordered antiferromagnets under an applied field perpendicular to the easily magnetized axis of magnetization.[2b,3b,3c] On the other hand, when B//a*, a sharp drop in χ_p was observed by lowering the temperature, suggesting that the a* direction is approximately parallel to the easily magnetized axis. Although the precise determination of the principal axes of the susceptibility tensor requires measurements of the angular dependence of the magnetic susceptibility, the observed anisotropy of the magnetic susceptibility is consisitent with the onset of an antiferromagnetic phase transition at the Neel temperature, $T_N = \sim 8$ K, in $DOT^{\cdot+}\cdot FeCl_4^-$.

The synthesis and clarification of the magnetic behavior in multispin systems based on these radical cation frameworks are currently in progress.

Acknowledgment. We would like to thank the Ministry of Education, Science, Sports, and Culture of Japan for a Grant for Scientific Research in a Special Field, No. 10146101) and financial support from Iketani Science and Technology Foundation (Grant 0191002-A). M. Kurtasu thanks of JSPS Research Fellowship for Young Scientist.

Supporting Information Available: X-ray crystallographic data in CIF format and tables of short contacts (Tables S1−S4). This material is available free of charge via the Internet at http://pubs.acs.org.

IC7012649

(10) Fisher, M. E. *Am. J. Physiol.* **1964**, *32*, 343−346.
(11) The Bonner−Fisher model using the alternating chain also gave similar values, −5.8 and −6.8 K.